

Ndubuisi Chimezie Nwachukwu<sup>1</sup>, Nnaemeka Princewill Ohia<sup>2</sup>,  
Stanley Toochukwu Ekwueme<sup>2</sup>

<sup>1</sup>Department of Process Engineering, University of Bremerhaven, Germany

<sup>2</sup>Department of Petroleum Engineering Federal University of Technology,  
Owerri, Nigeria

Scientific paper

ISSN 0351-9465, E-ISSN 2466-2585

<https://doi.org/10.62638/ZasMat1295>



Zastita Materijala 66 (4)

784 - 803 (2025)

## Response surface methodology and artificial neural networks optimisation of CO<sub>2</sub> methanation simulation using Ni/MgAl<sub>2</sub>O<sub>4</sub> catalyst in a multi-tubular fixed-bed reactor

### ABSTRACT

*This study investigated the simulation and optimization of synthetic methane production over Ni/MgAl<sub>2</sub>O<sub>4</sub> in a multi-tubular fixed-bed reactor. The study comprises process simulation conducted using Aspen HYSYS software, modelling and optimization using response surface methodology (RSM) and artificial neural network (ANN) modelling performed using Design Experts and MATLAB software, respectively. In the process simulation for the CO<sub>2</sub>methanation, sensitivity analyses were performed to determine the effects of temperature, pressure, H<sub>2</sub>/CO<sub>2</sub> ratio, and CO fraction in the feedstock on CO<sub>2</sub>conversion, CH<sub>4</sub> yield, and CH<sub>4</sub> selectivity. RSM and ANN models were built using datapoints provided by the process simulation results to model the relationship between input variables and output responses and perform optimisation for RSM model and ANN model coupled with genetic algorithm (GA). The process simulation results profoundly highlighted the impact of temperature in enhancing CO<sub>2</sub> conversion and CH<sub>4</sub> yield. Higher temperatures favoured the endothermic reversed water-gas shift (RWGS) reaction, leading to increased CO<sub>2</sub> conversion and CH<sub>4</sub> yield. CO<sub>2</sub> conversion, CH<sub>4</sub> selectivity and yield were found to be minimally affected by pressure. CO fraction in the feed was found to exert a delicate influence on the CO<sub>2</sub> conversion and CH<sub>4</sub> yield. Excessive CO fractions hindered the methanation process, reducing both CO<sub>2</sub> conversion and CH<sub>4</sub> yield. Additionally, the H<sub>2</sub>/CO<sub>2</sub> ratio proved critical as higher ratios facilitated higher CO<sub>2</sub> conversion, CH<sub>4</sub> selectivity, and yield, emphasizing the significance of optimal hydrogen to CO<sub>2</sub> ratio for efficient methanation which was proposed to be at values higher than the stoichiometric value of 4:1. Furthermore, the ANN-GA model outperformed RSM in terms of prediction accuracy and optimization. The ANN model demonstrated superior capabilities in capturing the complex relationships between the input variables and output responses demonstrated by the performance metrics including R<sup>2</sup> values, MSE, RMSE etc. The optimisation results of the ANN-GA model provided more precise and efficient predictions when compared with RSM, offering a deeper understanding of the intricate interactions within the methanation process.*

**Keywords:** Artificial Neural Networks, CO<sub>2</sub> Methanation, HYSYS Modelling, Response Surface Methodology, Reverse Water Gas Shift, Langmuir-Hinshelwood-Hougen-Watson Rate Expression

### 1. INTRODUCTION

Fossil fuels have served as a reliable and cost-effective energy source for centuries. The advent of the Industrial Revolution, driven by innovations like the internal combustion engine, led to remarkable scientific, technological, and industrial progress facilitated by the fossil fuel economy [1]. Nonetheless, fossil fuels face significant challenges, including dwindling reserves and the rise in anthropogenic carbon dioxide (CO<sub>2</sub>) emissions, making them less desirable in the face of global environmental concerns [2, 3].

The usage of fossil fuels contributes substantially to CO<sub>2</sub> emissions, a major greenhouse gas responsible for the climate issues we observe today, particularly global warming, which entails an increase in average global temperatures [4]. Global warming is a pressing global issue due to its potentially catastrophic consequences, necessitating urgent attention before it escalates into a pandemic [5].

Various strategies have been proposed for CO<sub>2</sub> reduction, such as enhancing energy efficiency, replacing fossil fuels with renewable or low-carbon energy sources, employing carbon capture and storage (CCS) technologies for CO<sub>2</sub> removal, and expanding the use of carbon conversion technologies that transform captured CO<sub>2</sub> into valuable fuels and chemicals [6]. The conversion of

\*Corresponding author: Stanley Toochukwu Ekwueme  
E-mail: stanleyekwueme@yahoo.com

Paper received: 11.11.2024.

Paper accepted: 06.01.2025.

captured CO<sub>2</sub> into value-added fuels and chemicals offers a unique solution to address global warming while providing synthetic fuels and chemicals. However, it's a challenging task to activate CO<sub>2</sub> and convert it into hydrocarbons or alcohols because CO<sub>2</sub> is a fully oxidized, thermodynamically stable, and chemically inert molecule [7]. Another challenge arises from the low C/H ratio achieved during CO<sub>2</sub> hydrogenation, primarily due to the relatively weak adsorption of CO<sub>2</sub> on catalyst surfaces. This weak adsorption promotes the rapid hydrogenation of surface-adsorbed intermediates, resulting in the formation of methane and a decrease in chain growth. Consequently, most research efforts have focused on selectively hydrogenating CO<sub>2</sub> into short-chain products, such as methanol, methane, C<sub>2</sub>-C<sub>4</sub> compounds, etc [8].

Among carbon conversion processes, synthetic natural gas (CH<sub>4</sub>) production through CO<sub>2</sub> hydrogenation, has received the most research focus, primarily due to its higher methane selectivity [7]. Producing synthetic natural gas (CH<sub>4</sub>) in this manner requires a substantial amount of hydrogen during the hydrogenation process. Hydrogen can be produced from renewable sources, such as water electrolysis or biomass, using renewable electricity (e.g., solar, wind) or from non-renewable means like fossil fuels (both as an energy and electricity source) [9]. Synthetic natural gas (CH<sub>4</sub>) serves as a crucial fuel source for numerous nations, offering a potential alternative to reduce dependence on Russian gas and contributing to environmental carbon balance by achieving net-zero carbon emissions [10].

The Sabatier reaction for synthetic natural gas (CH<sub>4</sub>) production occurs at temperatures ranging from 150-550°C and pressures from atmospheric to about 100 bars in fixed-bed or fluidized-bed reactors [4]. However, the exothermic nature of this process presents significant challenges, including limitations in achieving thermodynamic equilibrium and the formation of soot, which can deactivate catalysts and hinder the desired reaction product formation [11].

The Sabatier reaction faces challenges in both kinetics and thermodynamics. Thermodynamically, the best CO<sub>2</sub> conversion and methane selectivity (close to 100%) occur at low temperatures when appropriately designed low-temperature catalysts are used [1]. Higher temperatures, exceeding 550°C, can restrict CO<sub>2</sub> conversion due to thermodynamic equilibrium, while lower temperatures may hinder the reaction kinetics, resulting in low reaction rates [12, 13]. Hence, effective heat management and catalyst improvement are critical optimization routes for the Sabatier reaction process.

The exact reaction mechanism of the Sabatier process remains a subject of debate in the literature, particularly regarding the formation of carbon monoxide as an intermediate in the reaction [13, 14]. Two mechanisms are commonly proposed: a direct reaction of CO<sub>2</sub> with hydrogen to form methane and water or a mechanism involving the formation of intermediate carbon monoxide, followed by its conversion to methane [4]. The latter mechanism is widely accepted and forms the basis for this work.

Heterogeneous catalytic reactions are important in the chemical industry, with catalysts often sized into small pellets for use in reactors such as fixed-bed and multi-tubular fixed-bed reactors. However, this pelletization can lead to diffusion limitations and the development of concentration gradients within the pellets, particularly during methanation reactions [4]. Measuring spatial profiles within these catalyst pellets can be challenging, making modelling and simulation crucial for understanding the diffusion-reaction processes, which are essential for process design.

Synthetic methane production is a complex and multiparametric process influenced by various factors, including temperature, pressure, H<sub>2</sub>/CO<sub>2</sub> ratio, and GHSV (gas hourly space velocity). The optimisation of carbon conversion, methane yield, and methane selectivity is crucial for the improved process economics. Scholars have sought robust and cost-effective approaches to address this complexity. Response Surface Methodology (RSM) and Artificial Neural Networks (ANNs) have gained significant attention in this application [15].

Response surface methodology (RSM) is a powerful tool for predicting complex processes [16]. It includes principal design techniques such as the Box-Behnken design and central composite design. RSM is effective when modelling processes involving multiple variables [17]. RSM significantly reduces the number of experimental runs needed compared to the one-factor-at-a-time method and is capable of developing empirical models to describe processes. Its utility has been demonstrated in numerous applications, including CO<sub>2</sub> hydrogenation and methanation [15, 18].

Ali et al. [19] studied CO<sub>2</sub> methanation using M/Mn/Fe-Al<sub>2</sub>O<sub>3</sub> catalysts (M = Pd, Rh, & Ru). They observed that catalytic performance could be improved by enhancing varying process parameters such as operating temperature, gas hourly space velocity (GHSV), and feed composition. They optimized conditions with Response Surface Methodology (RSM), which emphasised the importance of loading. The best

catalyst observed was Ru/Mn/Fe-Al<sub>2</sub>O<sub>3</sub> (5:35:60 ratio, calcined at 1,000°C), achieving 96.1% CO<sub>2</sub> conversion and 66.0% CH<sub>4</sub> formation at 270°C. Optimal conditions included 5.5 wt % Ru loading, 1,010°C calcination, and 5 g catalyst loading, with 95.0% experimental CO<sub>2</sub> conversion which matched the 96.6% prediction.

Younas et al. [20] conducted a study on CO<sub>2</sub> methanation over Ni and Rh-based catalysts at lower temperatures. They optimized Rh-based catalysts for CO<sub>2</sub> methanation using RSM, achieving high CO<sub>2</sub> conversion (54.4%) and CH<sub>4</sub> selectivity (73.5%) at 206.7°C, 12.5% humidity, and 100 mg of the catalyst.

Zhang et al. [21] developed NiFe/(Mg,Al)O<sub>x</sub> catalysts for plasma-catalytic CO<sub>2</sub> methanation, with RSM revealing that higher voltage, lower gas flow, and higher H<sub>2</sub>:CO<sub>2</sub> ratio favoured selective CO<sub>2</sub> hydrogenation to CH<sub>4</sub>, reaching 84.7% CO<sub>2</sub> conversion and 100% CH<sub>4</sub> selectivity.

Artificial Neural Networks (ANNs) can model complex chemical and physical processes due to their ability to approximate arbitrary non-linear functions, generalization capacity, computational efficiency, and handling high-dimensional data. ANNs are modelled after the human brain and can effectively capture intricate nonlinear processes through built-in training algorithms, identifying relationships between dependent and independent variables [17].

In this study, ANNs/RSM was employed for modelling and optimizing CO<sub>2</sub> methanation in a multi-tubular fixed-bed reactor. There is to date no record of the use of ANN and RSM for the optimisation of CO<sub>2</sub> methanation production simulation process. This research aims to determine the suitability of RSM and ANN for process modelling and optimization while evaluating the process performance. Process modelling was conducted using HYSYS software, which provided data for subsequent statistical analysis.

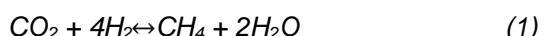
## 2. THEORETICAL CONCEPTS

### 2.1. CO<sub>2</sub> Methanation

French chemists Paul Sabatier and Jean-Baptiste Senderens studied the thermochemical CO<sub>2</sub> methanation reaction since 1902. This reaction involves the catalytic conversion of CO<sub>2</sub> to methane at high temperatures, utilizing a specially prepared catalyst and reacting it with hydrogen. An ongoing debate surrounds the pathway of synthetic methane formation during CO<sub>2</sub> methanation. The argument hinges on whether a CO intermediate is formed in the process [4, 9]. Two proposed pathways exist: some scholars propose that

methanation occurs directly through the hydrogenation of CO<sub>2</sub> to methane (see equation 1), while others suggest that a CO intermediate is first formed through a reverse water gas shift (RWGS) reaction. Subsequently, this CO reacts with hydrogen to produce methane (equations 2 and 3). However, the mechanism that involves the intermediate conversion to CO has been the most widely investigated [4].

The equations of reaction for the one-step and the two-step processes are given in equations 1, 2, and 3.



In the design and implementation of the Sabatier reaction, understanding thermodynamics is crucial. The CO<sub>2</sub> methanation reaction is highly exothermic, hence, operating at high temperatures can lead to reactor overheating, soot formation, and catalyst deactivation due to sintering [2, 22]. High temperatures shift the thermodynamic equilibrium towards the reactant side, resulting in lower CO<sub>2</sub> conversion, methane selectivity, and yield. Conversely, operating at lower temperatures favours the exothermic process and enables the achievement of optimal CO<sub>2</sub> conversion, methane selectivity, and yield of up to 100% [15, 23, 24]. However, low temperatures pose kinetic limitations because reaction rates are temperature-dependent [25]. Special low-temperature catalysts are required to overcome these kinetic barriers and increase reaction rates [26]. Avoiding temperatures above 550°C is advisable in the Sabatier process to prevent catalyst deactivation through sintering.

Operating at high pressures is favourable for achieving high CO<sub>2</sub> conversion, methane selectivity, and yield. Additionally, the H<sub>2</sub>/CO<sub>2</sub> molar ratios impact process performance, with higher ratios, especially above stoichiometric values, promoting higher CO<sub>2</sub> conversion while reducing carbon deposition [27]. Jürgensen et al. [28] found that higher pressures raise the temperature at which carbon deposition occurs. Their results showed carbon deposition at 365°C at 1 bar pressure but the deposition increased at 515°C when the pressure was raised to 11 bars.

### 2.2. CO<sub>2</sub> Methanation Feedstock Sources

In the production of synthetic methane through CO<sub>2</sub> methanation, the source of CO<sub>2</sub> and H<sub>2</sub> significantly affects the quality of the methane produced [29]. CO<sub>2</sub> can be sourced from power plants, industry, biomass, or air, while hydrogen is mainly produced through water

electrolysis, which is recommended for power-to-gas projects. CO<sub>2</sub> recovery methods vary based on the source, as impurity levels affect project costs[30]. Industrial sources offer higher CO<sub>2</sub> concentrations, making capture more cost-effective than power plants[31]. Air has the lowest CO<sub>2</sub> concentration and requires more advanced technology for extraction. CO<sub>2</sub> capture from power plants can occur at different combustion stages: pre-combustion (higher CO<sub>2</sub> concentration), post-combustion (lower CO<sub>2</sub> concentration, with impurities), and oxy-fuel (very high purity but higher oxygen requirement)[32]. Oxy-fuel yields purer CO<sub>2</sub> but at higher capture costs. After CO<sub>2</sub> capture, separation methods such as absorption, adsorption, chemical looping, membranes, and cryogenics are employed. Costs depend on the source, capture technique, power source, and process design[31].

Hydrogen for CO<sub>2</sub> methanation can come from coal gasification or water electrolysis. Electrolytic hydrogen, produced using renewable energy sources, aligns with sustainability goals but has high costs. Environmental regulations limit fossil fuel hydrogen use, focusing on electrolytic hydrogen[15]. Electrolytic hydrogen production is complex and energy-intensive and faces challenges such as low efficiency, material costs, and power density issues. Proper design and resource optimization are crucial for electrolytic hydrogen production. Three main types of electrolyzers exist: alkaline, polymer electrolyte membrane (PEM), and solid oxide electrolyser (SOE). Alkaline electrolysis has 77% efficiency, expected to reach 82% by 2050. PEM technology offers flexibility but uses expensive catalysts. SOE operates at high temperatures, potentially reaching 86% efficiency in the future[15].

### 2.3. CO<sub>2</sub> Methanation Reactor

CO<sub>2</sub> methanation is an exothermic reaction, which makes effective temperature control a critical consideration in the reactor design. Poor heat management can lead to temperature spikes within the catalyst bed which can exceed thermodynamic limits, and cause issues like hot spots, stress on construction materials, and catalyst sintering[33]. Elevated outlet temperatures can also limit CO<sub>2</sub> conversion due to thermodynamic equilibrium, resulting in a gas composition that does not meet natural gas grid specifications[34].

Catalytic methanation has been extensively explored in Power-to-Gas (PtG) applications. In this regard, the reactors are typically operated at temperatures ranging from 200 to 550°C and pressures from 1 to 20 bar. While methanation processes have long been used in industrial ammonia production and synthetic natural gas

(SNG) generation following the oil crises of the 1970s, their application in Power-to-Gas processes is more complex due to the smaller plant sizes and intermittent or dynamic operation[35].

CO<sub>2</sub> methanation reactors are generally categorized into two-phase and three-phase reactors, with two-phase reactors being more common for commercial applications. Various designs are used for two-phase reactor systems, including fixed-bed reactors (adiabatic or cooled), structural reactors, and fluidized-bed reactors[34].

Fixed-bed reactors, especially adiabatic fixed-bed reactors (AFBR), are frequently employed for CO<sub>2</sub> methanation. In these reactors, catalyst particles are packed in a stationary bed, and reactant gases flow through the bed. AFBRs are often operated at high pressures (above 20-30 bars) to favour thermodynamically favourable CH<sub>4</sub> production, but this can lead to high temperatures in the first reactor, necessitating thermally stable catalysts. However, these high temperatures can decrease methane production and potentially lead to local hot spots, reducing catalyst activity. AFBRs also suffer from low flexibility and high-pressure drop[35].

Several approaches have been developed to mitigate the temperature increase in the catalyst bed due to the exothermic nature of methanation. These include gas recirculation, catalyst dilution with inert materials, and intercooling stages between fixed-bed reactors. While effective, these solutions require additional equipment, increase reactor volume, and add complexity to the overall process, driving up construction and operating costs[36].

However, fixed-bed reactors constitute the highest level of technological maturity for CO<sub>2</sub> methanation. Leading suppliers in this field, such as Air Liquide (formerly Lurgi), Haldor Topsøe, and Johnson Matthey (Davy Technologies), offer adiabatic reactor-based methanation technologies[35]. However, it's important to note that the high pressure and temperature requirements of adiabatic fixed-bed reactors can result in significant construction and operating costs, including increased equipment wall thickness and higher compression power demands[37]. The maximum operating Gas Hourly Space Velocity (GHSV) for adiabatic fixed-bed reactors in technical plants typically falls within the range of 2000-5000 h<sup>-1</sup>[36].

Cooled Fixed Bed Reactors (CFBR) represent another technology used in methanation applications. CFBR systems typically consist of multi-tubular fixed-bed reactors or plate reactors. In comparison to Adiabatic Fixed Bed Reactors (AFBR), CFBR technology focuses on reducing the

temperature gradient between the gas inlet and outlet by incorporating heat transfer from the methanation reactor to a cooling medium [37]. Common cooling mediums include pressurized boiling water, steam, or thermal oil. However, even with cooling, temperature gradients persist within the catalyst bed, and hot spots cannot be completely avoided due to limited thermal transfer between the reaction zone and cooling surfaces. Additionally, challenges arise during catalyst conditioning and loading, which can lead to the formation of gas preferential paths due to potential heterogeneous catalyst distribution[36].

CFBRs are generally more complex and expensive compared to AFBRs [36] but the overall unit cost may not necessarily be higher than that of AFBR processes. Typically, two reactor stages are required to achieve the desired CO<sub>2</sub> conversion[34, 36]. Alternatively, designing longer reactors to ensure complete CO<sub>2</sub> conversion is an option, but this can result in the formation of hot spots and gradual catalyst deactivation, potentially causing variations in SNG quality and production[38].

Several companies offer fixed-bed reactor technologies on the market. For example, MAN provides a cooled fixed-bed reactor with molten salt cooling, Outotec offers a staged fixed-bed reactor with intermediate cooling, and Etogas utilizes fixed-bed or plate reactors with steam cooling [38].

Structured fixed-bed reactors represent technologies in development aimed at addressing the limitations of AFBRs, including temperature hot spots and high-pressure drops. These structured reactors and micro-reactors have certain drawbacks, such as high manufacturing costs and scalability challenges. Examples of structured reactors include honeycomb, microchannel, sorption-enhanced, and membrane reactors [36].

Microchannel reactors (MCRs) have been developed to enhance heat transfer and minimize hot spot formation within the methanation reactor by increasing the exchange area. MCRs consist of numerous channels with diameters in the micro-meter range. A microchannel CO<sub>2</sub> methanation pilot reactor was tested at the Laziska power plant in Poland [39], divided into two stages, and operated at pressures of around 1–3 bars and temperature of 300 °C. The maximum CO<sub>2</sub> conversion achieved was 98%, resulting in SNG composed of methane (82%), hydrogen (13%), and carbon dioxide (5%). Industrial upscaling remains a significant challenge for MCRs, primarily due to their high costs [40]. It's worth noting that once the catalyst is deactivated, the entire microchannel reactor must be replaced. Additionally, a temperature gradient of approximately 260°C

gradually moves within the reactor with catalyst deactivation, promoting catalyst sintering [37].

Fluidized Bed Reactors (FBRs) represent another technology used in methanation applications. These reactors involve the suspension of catalyst particles in the reactor through upward-flowing gases, mimicking fluid-like behaviour. Catalyst particles are fluidized by the gas flow, ensuring uniform contact with reactants. CO<sub>2</sub> and H<sub>2</sub> are introduced, and methane forms on the catalyst surface[41]. One of the key advantages of FBRs, when compared to other catalytic technologies, is the nearly homogeneous temperature distribution in the catalytic bed, owing to their exceptional heat transfer characteristics. To manage the exothermic nature of methanation, internal heat exchangers can be integrated into the bed to precisely control the reaction temperature[42]. As a result, hot spots and catalyst sintering are entirely avoided. Due to the high heat transfer coefficient between the fluidized bed and tube wall (typically ranging from 100 to 400 W/m<sup>2</sup>·K) [41,42]. The size and capacity of internal heat exchangers are significantly smaller than those for CFBR [36]. Efficient solid mixing is also achieved in fluidized beds, which plays a pivotal role in the observed behaviour.

One notable feature of FBRs is their high flexibility concerning inlet flowrate (1–4 factor), essential for PtM applications to manage variations in inlet flowrate. However, designing FBRs can be challenging due to the need to provide sufficient exchange area between the fluidized bed and the exchanger tubes to handle heat generated by exothermic reactions. The gas volume contraction during methanation reactions necessitates low bed diameters to ensure bed fluidization, imposing stringent design constraints on internal heat exchangers. To address this, options include increasing fluidized bed height or reducing catalyst particle size[41]. FBRs can also be operated at high temperatures (>450 °C) to enhance the heat transfer coefficient and limit the amount of heat to be extracted. However, operating at such high temperatures is thermodynamically unfavourable for CO<sub>2</sub> conversion. Alternatively, FBRs can be operated at low pressure (2–5 bar) to increase the volumetric flowrate and enhance the heat exchange area. This approach also reduces overall gas compression costs since pressurization occurs with the product gas (which has a much lower volumetric flowrate than the reactant gas) rather than the inlet gas. While low pressure is unfavourable for the methanation reaction, thermodynamic analysis indicates that pressure has minimal impact on methanation at low temperatures (250–350 °C) [27].

Three-phase methanation represents a distinct catalytic process characterized by highly dynamic operability. Slurry Bubble Column Reactors (SBCR) serve as a prime example of a three-phase reactor for CO<sub>2</sub> methanation. SBCRs achieve effective heat management with homogeneous temperatures throughout the methanation reactor. In SBCRs, the catalyst is suspended in a liquid solution. However, it's essential to limit the catalyst's concentration to maintain an adequate gas-liquid mass transfer rate [34], which is the rate-limiting step in SBCRs. As catalyst dilution increases, reactor volume expands compared to fixed bed and fluidized bed reactors. SBCR performance has been demonstrated to significantly improve with higher pressures [34]. Consequently, achieving high CO<sub>2</sub> conversion in SBCRs demands substantial compression costs. However, the Capital Expenditure (CAPEX) of this technology is notably lower than AFBRs or CFBRs, primarily because it requires less equipment [43].

#### 2.4. Aspen HYSYS Modelling Concepts

Aspen HYSYS is a powerful process simulation software with a wide range of applications in chemical engineering and sustainable energy production. When utilized for CO<sub>2</sub> methanation, it provides critical capabilities for modelling and optimisation. HYSYS offers a utility environment to define and tailor reaction kinetics models for CO<sub>2</sub> methanation, allowing precise control over reactants, reaction rates, and methane formation. The predictions of the behaviour of the reactants under varying temperature and pressure conditions are achieved through established thermodynamic models and databases[44]. Aspen HYSYS facilitates the creation of detailed process flow diagrams (PFDs) for CO<sub>2</sub> methanation reactors, enabling comprehensive simulations ranging from feed input to product separation. Engineers can utilize Aspen HYSYS to transition from laboratory-scale processes to industrial-scale operations[45]. It aids in the design of larger reactors, efficient heat management, and ensures compliance with safety considerations. Aspen HYSYS offers users the possibility to choose from its inbuilt reaction library which includes conversion reactions, equilibrium reactions, Gibbs reactions, kinetic reactions, heterogeneous catalytic reactions, etc. However, reactions more akin to CO<sub>2</sub> methanation include the kinetic and the heterogenous catalytic reaction types[45].

Aspen HYSYS also supports comprehensive cost estimation and economic analysis, including capital expenditures (CAPEX) and operating expenses (OPEX). This capability is necessary for evaluating the feasibility and profitability of CO<sub>2</sub> methanation projects.

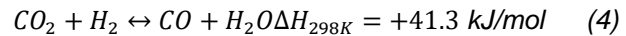
### 3. METHODOLOGY

The methodology comprises Process modelling and simulation, RSM modelling, and the ANN modelling. The process simulation was used to build the process model for the hydrogenation of CO<sub>2</sub> to methane. The process results subsequently served as input for the RSM and ANN modelling.

#### 3.1. Process Modelling and Simulation

##### 3.1.1. Kinetic model

Kinetics are given for each of the catalysed reactions that occur in the methanation process. The two-step methanation process comprises the intermediate production of CO and the subsequent hydrogenation of CO to methane. This is summarised in the equations of reaction given in equations 4 and 5 respectively.



Equation 4 relates to the reversed water gas shift reaction (RWGS) while equation 4 is the CO methanation reaction. The overall process is exothermic and is investigated at temperature ranges of 300°C to 500°C and pressures of up to 100 bars.

The kinetic model used for the process simulation of methane production through CO<sub>2</sub> methanation is that given by Xu and Froment [46] over Ni/MgAl<sub>2</sub>O<sub>4</sub> catalyst. This model is presented following the Langmuir-Hinshelwood-Hougen-Watson (LHHW) rate expression, the rate constant and the adsorption parameters are defined by the Arrhenius type expression. The mechanism of the CO<sub>2</sub> conversion considered is the indirect route wherein CO<sub>2</sub> is first converted to CO by reversed water gas shift reaction and the subsequent hydrogenation of the CO to methane. This two-step process is performed in separate reactors.

The kinetic model given by Xu and Froment [46] for Ni/MgAl<sub>2</sub>O<sub>4</sub> catalyst is given as:

$$R_1 = \frac{\frac{k_1}{p_{H_2}}(p_{H_2}p_{CO_2} - \frac{p_{CO}p_{H_2O}}{K_{eq1}})}{\left(1 + K_{cop}p_{CO} + K_{H_2}p_{H_2} + K_{CH_4}p_{CH_4} + K_{H_2O}\frac{K_{H_2O}}{p_{H_2}}\right)^2} \quad (6)$$

$$R_2 = \frac{\frac{k_2}{p_{H_2}^{2.5}}(p_{H_2}^{2.5}p_{CO} - \frac{p_{CH_4}p_{H_2O}}{K_{eq2}})}{\left(1 + K_{cop}p_{CO} + K_{H_2}p_{H_2} + K_{CH_4}p_{CH_4} + K_{H_2O}\frac{K_{H_2O}}{p_{H_2}}\right)^2} \quad (7)$$

Where R<sub>1</sub> and R<sub>2</sub> represent the kinetic rate model for the RWGS reaction and the CO methanation reaction respectively.

The equilibrium constants K<sub>eq1</sub> and K<sub>eq2</sub> are given as:

$$K_{eq1} = \exp\left(\frac{4400}{T} - 4.036\right) \quad (8)$$

$$K_{eq2} = \exp\left(\frac{-26830}{T} + 30.114\right) \quad (9)$$

The kinetic factor (rate constant) is expressed using Arrhenius and Vant Hoff's expression in Equation 10 and 11

$$k_i = k_{i,0} \exp\left(-\frac{E_{A,i}}{RT}\right) \quad (10)$$

$$K_j = K_{j,0} \exp\left(-\frac{\Delta H_j}{RT}\right) \text{ for } j = A, B, \text{ and } P \quad (11)$$

$k_i$  is the rate constant,  $\text{mmol}^{-1}\text{min}^{-1}\text{bar}^{-2.5}$

$k_{i,0}$  is the pre-exponential factor,  $\text{mmol}^{-1}\text{min}^{-1}\text{bar}^{-2.5}$

$K_j$  is the adsorption rate constant,  $\text{mmol}^{-1}\text{min}^{-1}\text{bar}^{-2.5}$

$K_{j,0}$  is the pre-exponential factor for the adsorption rate constant,  $\text{mmol}^{-1}\text{min}^{-1}\text{bar}^{-2.5}$

$\Delta H_j$  is the adsorption enthalpy change,  $\text{kJ/mol}$

$T$  is the temperature in kelvin

The kinetic parameters corresponding to the pre-exponential factors, the activation energy, and the adsorption parameters are given in Table 1

The  $\text{CO}_2$  conversion, methane selectivity, and yield were calculated using the following equations.

$$\text{CO}_2 \text{ Conversion: } X_{\text{CO}_2} (\%) = \frac{V_{\text{CO}_2,\text{in}} - V_{\text{CO}_2,\text{out}}}{V_{\text{CO}_2,\text{in}}} \times 100 \quad (12)$$

$$\text{CH}_4 \text{ Selectivity: } S_{\text{CH}_4} (\%) = \frac{V_{\text{CH}_4,\text{out}}}{V_{\text{CH}_4,\text{out}} + V_{\text{CO},\text{out}}} \times 100 \quad (13)$$

$$\text{CH}_4 \text{ Yield: } Y_{\text{CH}_4} (\%) = \frac{V_{\text{CH}_4,\text{out}}}{V_{\text{CO}_2,\text{in}}} \times 100 \quad (14)$$

Table 1. Kinetic parameter for  $\text{Ni}/\text{MgAl}_2\text{O}_4$  catalyst

Parameter	Value	Unit
$k_1$	5.43E2	$\text{Mol}\text{bar}^{-0.5}\text{s}^{-1}$
$E_1$	67.13	$\text{kJ/mol}$
$k_2$	1.1736E12	$\text{Mol}\text{bar}^{-0.5}\text{s}^{-1}$
$E_2$	240.1	$\text{kJ/mol}$
KCO	8.23E-5	-
$\Delta H_{\text{CO}}$	-70.65	$\text{kJ/mol}$
KCH <sub>4</sub>	6.65E-4	-
$\Delta H_{\text{CH}_4}$	-38.28	$\text{kJ/mol}$
KH <sub>2</sub>	6.12E-9	-
$\Delta H_{\text{H}_2}$	-82.9	$\text{kJ/mol}$
KH <sub>2</sub> O	1.77E5	-
$\Delta H_{\text{H}_2\text{O}}$	88.68	$\text{kJ/mol}$

### 3.1.2. Process Simulation

The process simulation was conducted using Aspen HYSYS V11 software and Peng Robinsons fluid property package. The simulation begins with the methanation unit where the  $\text{CO}_2$  and hydrogen are reacted to produce methane by an indirect CO pathway. First  $\text{CO}_2$  was converted to CO and then the CO was methanated. Methane upgrading followed the methanation process where high purity methane was obtained by separation process which removed impurity gases from product gases.

The synthetic methane production block diagram is given in Figure 1

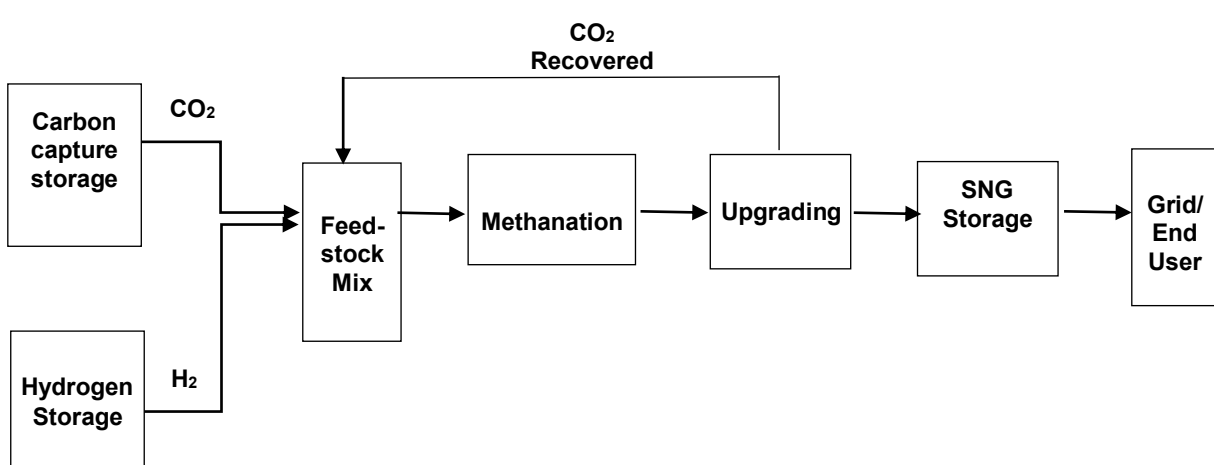


Figure 1. Block diagram of the synthetic methane production process

Sensitivities enable optimization of the process by investigating the effects of changes in several process parameters on the simulation results. This

will enable the determination of the best conditions to operate the plants based on the results obtained.

The input data used in this simulation includes the feed data, the reactor data, and catalyst data

Table 2. Input data used for the simulation

Parameter	Value	Unit
Inlet flowrate of H <sub>2</sub>	3494	kgmol/hr
Inlet pressure of H <sub>2</sub>	40	bar
Inlet temperature of H <sub>2</sub>	30	°C
Inlet flowrate of CO <sub>2</sub>	1494	kgmol/hr
Inlet pressure of CO <sub>2</sub>	40	bar
Inlet temperature of CO <sub>2</sub>	30	°C

The reactor and catalyst parameters are given in Table 3

Table 3. Reactor and catalyst data

Parameter	Value
Length of tube	12.07 m
Number of tubes	67500
Diameter of tube	0.025 m
Wall thickness	0.005 m
Total Reactor tube Volume	400 m <sup>3</sup>
Void fraction	0.45
Solid density of catalyst	1010 kg/m <sup>3</sup>
Diameter of catalyst particle	0.001 m

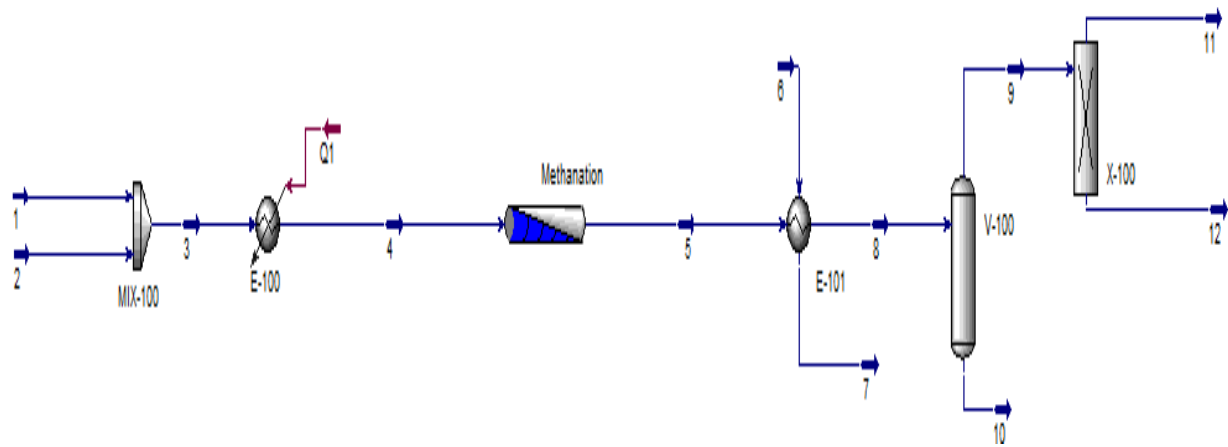


Figure 2. Process flow diagram (PFD) of the methanation unit

### 3.1.3. Simulation Description

The methanation process comprises the methanation and the upgrading. In HYSYS, a plug flow reactor was used for the simulation because it mostly represents a multi-tubular fixed-bed reactor.

Because the kinetics were expressed as LHHW expression, a heterogenous catalytic reaction type was selected for the reactions. The methanation process flow diagram (PFD) is given in Figure 2

Table 4. Material and energy stream description of the PFR

Stream	Description	T, oC	P, bar	Total	Duty, kW
1	Hydrogen	30	30	3486.5	-
2	CO <sub>2</sub>	40	26.55	1494.2	-
3	Mixed stream	30	40	4980.7	-
4	Reactor inlet	1000	40	4980.7	-
5	RWGS outlet	813.3	40	4980.7	-
6	RSMR outlet	900	40	3372.9	-
7	Warm water	30	1.01	200000	-
8	Hot water	98.55	0.9632	200000	-
9	Cooled reactor product	32	39.95	3372.9	-
10	Separated water	32	39.95	1849.7	-
11	Raw synthetic methane	32	39.95	1521	-
12	Compressed SNG (to dehydration)	75.76	62	1521	-
Q1	Heater duty	-	-	-	4836
Q2	Heat removed from reactor	-	-	-	4643
Q3	Compressor duty	-	-	-	608.7

The methanation process begins with the introduction of the feedstock  $\text{CO}_2$  (stream 1) and hydrogen (stream 2) from two lines at 40 bar pressure and 30°C temperature respectively. A mixer was placed upstream of the feedstock inlet to mix the incoming stream and send the mixed stream (stream 3) to a heater. The heater raises the temperature of the mixed stream from 30°C to 1000°C pressure suitable for the reactor environment. The RWGS reactor was operated adiabatically while the CO methanation reactor was operated isothermally with appropriate heat management. An upper-temperature limit of 1028°C was set for the CO methanation reactor to avoid reactor overheating and catalyst deactivation by sintering. The resulting products from the reactors comprise methane,  $\text{CO}_2$ , CO, hydrogen, and water which have to be processed to remove impurities and obtain methane of higher purity. Table 4 shows the material and energy stream description of the PFR.

### 3.2. RSM Modelling

The sensitivity results obtained from the process simulation served as experimental data which were used as input data for the RSM modelling. A Box-Behnken design (BBD) was used to develop the experimental plan as was implemented using Design Experts. The BBD was chosen for this study because it is suitable for modelling quadratic response surfaces which are typically encountered in most chemical engineering processes. Four variables (temperature, pressure,  $\text{H}_2/\text{CO}_2$  ratio, and CO fraction) that were observed to influence methane production were investigated. Furthermore, two output variables:  $\text{CO}_2$  conversion and methane yield were investigated. 30 experimental runs were produced by the BBD which was used for the modelling. Various regression analysis models were tested to select the most accurate one approximating the experimental data. The two-factor interaction (2FI) model performed best for  $\text{CO}_2$  conversion, while the quadratic model was optimal for methane yield. These models were chosen based on statistical parameters such as  $R^2$ , adjusted  $R^2$ , predicted  $R^2$ , standard deviation, and coefficient of variance (COV). Multiple regression analyses enabled the fitting of these models to the experimental data, allowing the estimation of responses from independent variables using the general equations given below:

The general form of the 2FI regression model is given as:

$$y = a_o + \sum_{i=1}^k a_i x_i + \sum_{i=1}^k \sum_{j < i} a_{ij} x_i x_j + e \quad (15)$$

The general form of the quadratic regression model is given as:

$$y = a_o + \sum_{i=1}^k a_i x_i + \sum_{i=1}^k \sum_{j=1}^k a_{ij} x_i x_j + \sum_{i=1}^k a_{ii} x_i^2 + e \quad (16)$$

Where  $x_i, x_j, x_l$  are the input variables and  $a_i, a_{ij}, a_{ii}$ , and  $a_{ijl}$  are the coefficient of each of the terms,  $a_o$  is the offset and  $e$  is the residual or error term,  $k$  is the number of input variables.

### 3.3. ANN Modelling

MATLAB software was used to develop artificial neural network (ANN) models to determine the relationship between the input variables and the output data and perform predictions for methane production. The ANN model was designed and modelled utilising data from process simulation sensitivity analyses results.

The ANN model was built in MATLAB using MATLAB's snntool. ANN model in MATLAB has several network architectures, training models, transfer functions, and optimal number of neurons. This ANN model implemented in this study comprises feed-forward neural network architecture based on the back propagation learning principle. The selected training model was the Levenberg-Marquardt (trainlm) while the transfer function was the tangent sigmoid (TANSIG) because they have demonstrated higher accuracy during predictions in literature. The topology of the multilayer perceptron (MLP) ANN structure input consists of five parameters, a hidden layer consisting of 15 neurons, and an output. The four-parameter input comprises temperature, pressure,  $\text{H}_2/\text{CO}_2$  ratio, and CO fraction. The ANN model was trained distinctively for the  $\text{CO}_2$  conversion and the  $\text{CH}_4$  yield. This was done because it provided higher performance than when the two outputs were combined in a single training model. Thus, the first ANN model training comprised  $\text{CO}_2$  conversion ( $R_1$ ) as the output while the second ANN training comprised  $\text{CH}_4$  yield ( $R_2$ ) as the output with the same input factors for both trainings. The ANN architecture is given in Figure 3.

Several trainings of the model were accomplished and the run with the best performance was selected. The criteria for selection were based on the  $R$ -value, the  $R^2$  value; mean squared error (MSE). Other statistical test parameters such as root mean squared error (RMSE), standard deviation; mean absolute error (MAE), and mean absolute percentage error (MAPE) were calculated to assess the accuracy of the prediction.

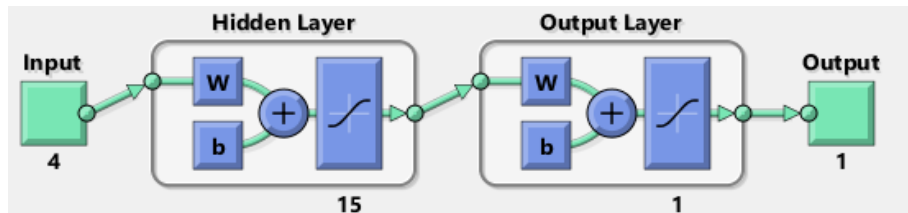


Figure 3. ANN architecture for each training

### 3.4. Optimisation

The  $\text{CO}_2$  conversion and  $\text{CH}_4$  yield were separately optimised using the RSM model and ANN model coupled with a genetic algorithm (GA). Thus, two optimisations were performed, RSM optimisation was performed using a built-in optimisation algorithm in Design Experts software while ANN model optimisation was done using the ANN fitness function coupled with GA toolbox in MATLAB.

### 3.5 Performance Metrics

Some statistical metrics are used to assess the performance of the RSM and ANN models developed. These comprise the coefficient of determination ( $R^2$ ), the mean-square error (MSE), the root-mean-square error (RMSE), the mean absolute error (MAE), the mean absolute percentage error (MAPE) and the standard deviation. The formulas for these statistical parameters are given below

$$R^2 = \frac{\sum_{i=1}^n (x_{a,i} - \bar{x}_{a,i})^2}{\sum_{i=1}^n (x_{p,i} - \bar{x}_{a,i})^2} \quad (17)$$

$$MSE = \frac{1}{n} \sum_{i=1}^n (x_{p,i} - x_{a,i})^2 \quad (18)$$

$$RMSE = \sqrt{\frac{1}{n} \sum_{i=1}^n (x_{p,i} - x_{a,i})^2} \quad (19)$$

$$MAE = \frac{1}{n} \sum_{i=1}^n |(x_{a,i} - x_{p,i})| \quad (20)$$

$$MAPE = \frac{\frac{1}{n} \sum_{i=1}^n |(x_{a,i} - x_{p,i})|}{\frac{1}{n} \sum_{i=1}^n x_{a,i}} \quad (21)$$

$$stddev = \sqrt{\frac{\sum_{i=1}^n (x_{d,i} - \bar{x}_d)^2}{n-1}} \quad (22)$$

Where  $n$  is the number of experimental runs,  $x_{p,i}$  is the estimated values,  $x_{a,i}$  is the experimental values,  $x_{a,ave}$  is the average experimental values,  $x_{d,i}$  is the difference between the actual and estimated value,  $m$  is the mean value of  $x_d$  dataset

## 4. RESULTS

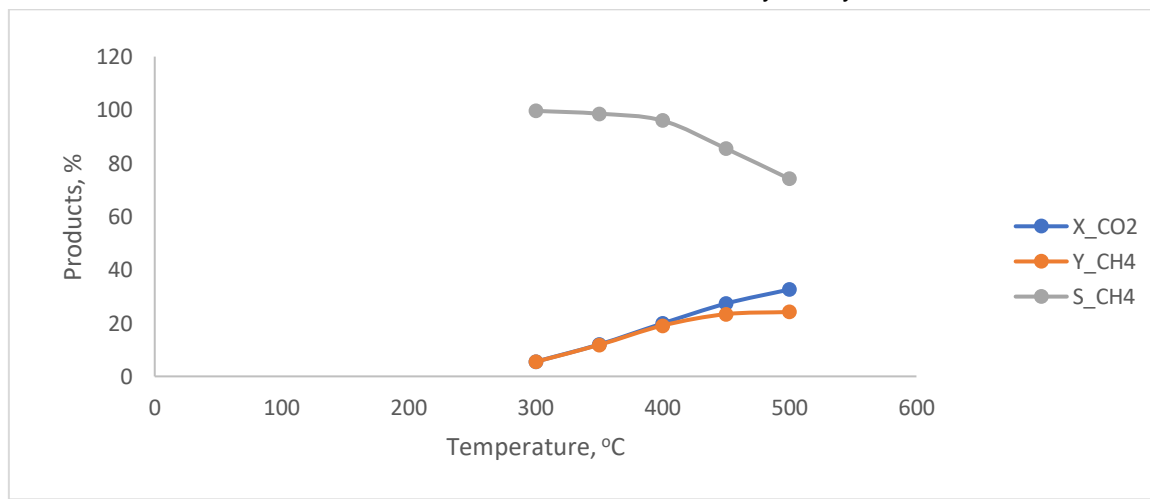
From the simulations performed, process simulation results, RSM simulation, and ANN simulation results are presented.

### 4.1. Process Simulation Results

The process simulation investigated the effect of input variables such as temperature, pressure,  $\text{H}_2/\text{CO}_2$  ratio, and CO fraction on  $\text{CO}_2$  conversion,  $\text{CH}_4$  selectivity, and  $\text{CH}_4$  yield. base process conditions included temperature of 500°C, pressure of 50 bars,  $\text{H}_2/\text{CO}_2$  ratio of 2.33 (which represent 70% mole ratio of  $\text{H}_2$  and 30% mole ratio of  $\text{CO}_2$ ),

#### 4.1.1. Effect of temperature

The effect of temperature on the methanation process was investigated for temperature ranges of 300°C to 500°C as shown in Figure 4. The effect of temperature was investigated for  $\text{CO}_2$  conversion,  $\text{CH}_4$  selectivity, and yield.

Figure 4. Effect of temperature on  $\text{CO}_2$  conversion,  $\text{CH}_4$  selectivity and yield for 50 bar pressure and  $\text{H}_2/\text{CO}_2$  ratio of 2.33

From Figure 4, it can be observed that  $\text{CO}_2$  conversion and  $\text{CH}_4$  yield increased with an increase in temperature while the  $\text{CH}_4$  selectivity decreased with an increase in temperature. Although in overall, methanation reaction is a net exothermic process, the initial RWGS reaction wherein the  $\text{CO}_2$  was converted to intermediate CO was however slightly endothermic as seen in equation 1. According to Le Chetallier's principle, an increase in temperature favour endothermic reaction by facilitating the forward reaction for producing the products. The  $\text{CO}_2$  conversion in the RWGS reaction was favoured at higher temperatures. Similarly, the  $\text{CH}_4$  yield also has similar temperature dependence as the  $\text{CH}_4$  yield increased with an increase in temperature. In the low-temperature regions (below 400°C), the values for the  $\text{CH}_4$  yield coincided with the values of  $\text{CO}_2$  conversion for each temperature. This indicates the high selectivity of the nickel-based catalyst at low temperatures. As can be seen, the selectivity was

higher than 95% for temperatures below 400°C, but as temperature increased, the selectivity began to decrease. A steep decrease in the  $\text{CH}_4$  selectivity was observed in the temperature ranges of 400°C to 500°C. The lower selectivity of  $\text{CH}_4$  at higher temperatures was due to the low conversion of CO to methane as the temperature was increased. Note that the CO methanation reaction is a highly exothermic process and proceeds to favour the production of the reactants at higher temperatures. Thus, slowed conversion of CO to methane at higher temperatures decreased the selectivity of methane and also explained the reason why the  $\text{CH}_4$  yield became lower than the  $\text{CO}_2$  conversion in the higher temperature ranges (400°C to 500°C).

#### 4.1.2. Effect of Pressure

The effect of pressure on the  $\text{CO}_2$  conversion,  $\text{CH}_4$  selectivity, and yield was investigated for pressures ranging from 50 bars to 100 bars, as shown in Figure 5

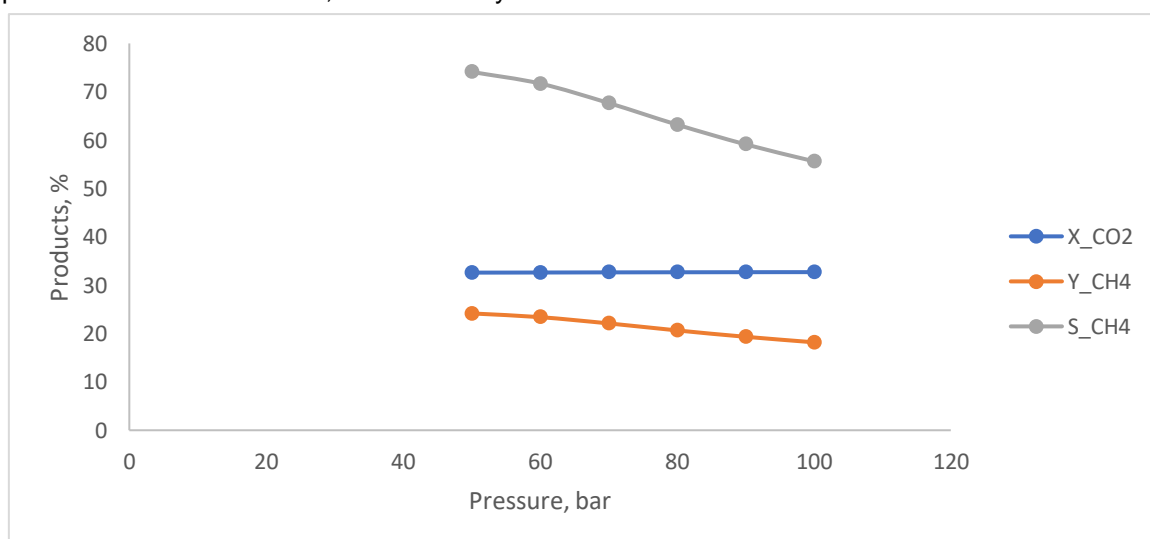


Figure 5. Effect of pressure on  $\text{CO}_2$  conversion,  $\text{CH}_4$  selectivity yield at 500°C, and  $\text{H}_2/\text{CO}_2$  ratio of 2.33

From Figure 5, it can be observed that pressure did not have a significant effect on the  $\text{CO}_2$  conversion. The  $\text{CO}_2$  conversion was almost constant with pressure increase as only minimal increase was observed. Meanwhile, the  $\text{CH}_4$  selectivity and  $\text{CH}_4$  yield decreased with increasing pressure. Moreover, similar to  $\text{CO}_2$ , conversion the effect of pressures on  $\text{CH}_4$  yield was less profound. The RWGS was a slightly endothermic reaction and would favour the production of products at higher pressures which explains the reason for the slight increase in  $\text{CO}_2$  conversion at higher pressures. Conversely, CO methanation was responsible for the production of methane is exothermic and prohibits the formation of methane

at higher pressures which explains the low methane yield and selectivity at higher pressures. Note that selectivity decreased steeply as pressure was decreased. Selectivity decreased from 74.1% at 50 bars to 55.6% at 100 bars at a constant temperature of 500°C.

The steep decrease in selectivity as pressure decreases can be explained by the shifting of the reaction equilibrium. At lower pressures, the equilibrium favours the formation of fewer products, leading to higher  $\text{CH}_4$  selectivity. This shift in equilibrium is especially notable at the high-temperature condition of 500°C. Lower pressures allow the reverse reaction (methane decomposing back to CO) to dominate, reducing the overall selectivity for methane.

#### 4.1.3 Effect of H<sub>2</sub>/CO<sub>2</sub> Ratio

The H<sub>2</sub>/CO<sub>2</sub> ratio was determined by dividing the molar flow rate of H<sub>2</sub> by the molar flowrate of CO<sub>2</sub>. Investigation of the effect of the H<sub>2</sub>/CO<sub>2</sub> ratio is important because the ratio of the molar flowrate of the feedstocks affects the species available for reaction. If there is not enough hydrogen gas to sufficiently hydrogenate the CO<sub>2</sub> and CO, then the conversion of CO<sub>2</sub> and yield of methane would be

limited. Theoretically, 4 moles of H<sub>2</sub> are required for every mole of CO<sub>2</sub> for the general equation of the methanation reaction. However, in a practical sense, the effect of the H<sub>2</sub>/CO<sub>2</sub> ratio on the methane product is influenced by other process variables. Figure 6 shows the effect of the H<sub>2</sub>/CO<sub>2</sub> ratio on the CO<sub>2</sub> conversion, CH<sub>4</sub> selectivity, and yield.

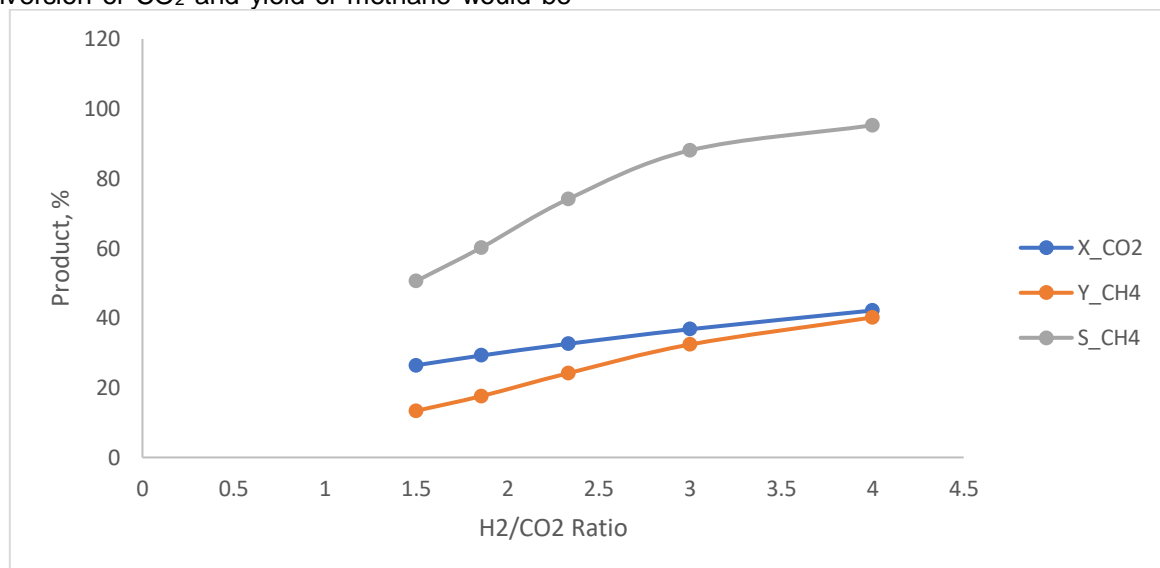


Figure 6. Effect of H<sub>2</sub>/CO<sub>2</sub> ratio on CO<sub>2</sub> conversion, CH<sub>4</sub> selectivity and yield at 50 bar pressure and 500°C temperature

It can be observed from Figure 6 that the CO<sub>2</sub> conversion, CH<sub>4</sub> selectivity, and CH<sub>4</sub> yield increased with an increase in H<sub>2</sub>/CO<sub>2</sub> ratio. This is attributed to the fact that at higher values of the H<sub>2</sub>/CO<sub>2</sub> ratio, more hydrogen was available for the hydrogenation of CO<sub>2</sub> and CO to form CO via RWGS and CH<sub>4</sub> via CO methanation respectively. However, it can also be observed that as the H<sub>2</sub>/CO<sub>2</sub> ratio increased the difference between the values of the CO<sub>2</sub> conversion and the CH<sub>4</sub> yield became smaller. The CO<sub>2</sub> conversion increased from 26.43% at H<sub>2</sub>/CO<sub>2</sub> ratio of 1.5:1 to 42.14% at H<sub>2</sub>/CO<sub>2</sub> ratio of 4:1. Similarly, the CH<sub>4</sub> yield increased from 13.37% at H<sub>2</sub>/CO<sub>2</sub> ratio of 1.5:1 to 40.14% at H<sub>2</sub>/CO<sub>2</sub> ratio of 4:1, while the CH<sub>4</sub> selectivity increased from 50.59% at H<sub>2</sub>/CO<sub>2</sub> ratio of 1.5:1 to 95.25% at H<sub>2</sub>/CO<sub>2</sub> ratio of 4:1. However, there would be a saturation point where further increasing the H<sub>2</sub>/CO<sub>2</sub> ratio might not significantly increase methane yield. Judging from Figure 6, the saturation point is at values slightly higher than the theoretical H<sub>2</sub>/CO<sub>2</sub> ratio of 4:1.

#### 4.1.4. Effect of CO Fraction

The source of the feed CO<sub>2</sub> might contain some fractions of CO or in some cases, CO may be

intentionally introduced into the feed. This is usually the case in mixed CO/CO<sub>2</sub> methanation. It is important to investigate the effect of fractions of CO in the feed on the CO<sub>2</sub> conversion, CH<sub>4</sub> selectivity, and yield. Figure 7 shows the effect of several fractions of CO in the feed ranging from 0.06 to 0.12 on the CO<sub>2</sub> conversion, CH<sub>4</sub> selectivity, and yield at temperature, pressure, and H<sub>2</sub>/CO<sub>2</sub> ratio of 500°C, 50 bars and 2.33:1.

From Figure 7, it can be observed that CO<sub>2</sub> conversion decreased with an increase in the fraction of CO in the feed. This is because as the fraction of CO in the feed increases, less CO<sub>2</sub> would be available for conversion. Meanwhile, the CH<sub>4</sub> yield and selectivity also showed a decreasing trend with an increase in the fraction of CO in the feed from 0.06 up to 1.0. At a CO fraction of 1.2, the CH<sub>4</sub> yield and selectivity were observed to suddenly slightly increase. The interpretation of this is that the rate of CO accumulation did not correspond to the rate of CO methanation in the formation of methane. More CO accumulated in the reactor as the CO fraction increased and the rate of CO methanation was not able to meet up with the accumulated CO at the reaction conditions of pressure, temperature, and H<sub>2</sub>/CO<sub>2</sub> ratio.

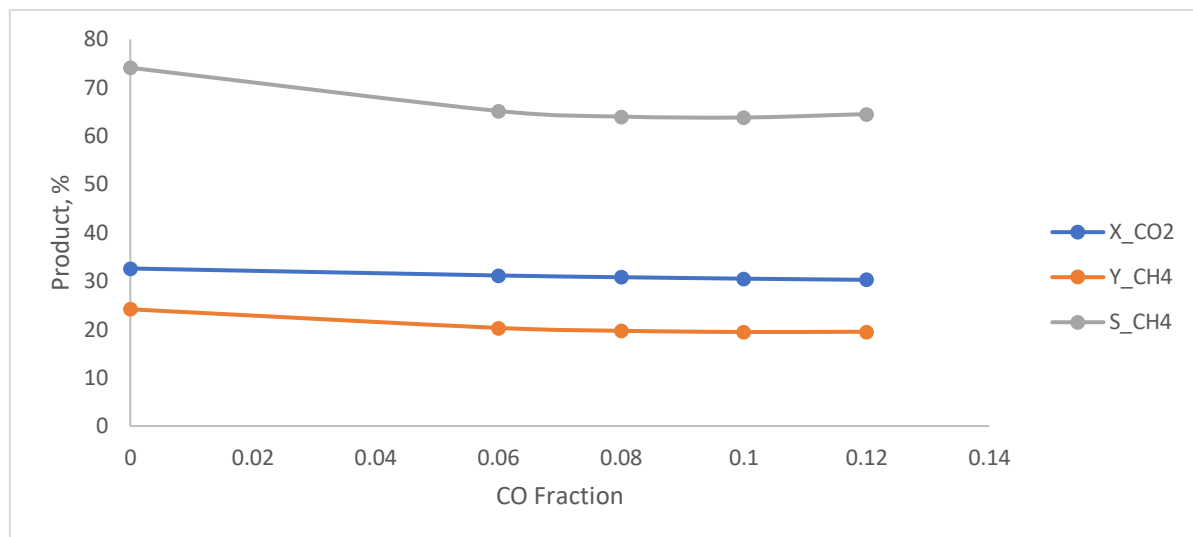


Figure 7. Effect of CO fraction in feed on CO<sub>2</sub> conversion, CH<sub>4</sub> selectivity, and CH<sub>4</sub> yield

#### 4.2. RSMM Modelling Results

The results of the RSM modelling are presented and discussed in this section. These results are shown in Table 5 and include the actual output from the process simulation and the corresponding predicted output responses from RSM for the input variables (which are the temperature, pressure, H<sub>2</sub>/CO<sub>2</sub> ratio, and CO fraction). For the process to be optimised, an RSM model had to be developed first. This was

accomplished by fitting the experimental data (from process simulation) to the RSM model. The regression model that gave the best fit to the actual data was selected. The 2FI model gave the highest fit to the actual data for CO<sub>2</sub> conversion while the quadratic model gave the best fit to the actual data for CH<sub>4</sub> yield and were selected respectively due to their best prediction accuracy. The equation for the 2FI model generated by RSM for the CO<sub>2</sub> conversion is given as:

$$\begin{aligned} \text{CO}_2 \text{ Conversion} = & +17.4 + 16.3X_1 + -0.7314X_2 + 4.34X_3 - 2.74X_4 - 0.0991X_1X_2 - \\ & -4.14X_1X_3 - 0.8329X_1X_4 - 0.32X_2X_3 - 0.385X_2X_4 - 0.505X_3X_4 \end{aligned} \quad (23)$$

As can be seen from the equation, the CO<sub>2</sub> conversion was influenced by temperature, pressure, H<sub>2</sub>/CO<sub>2</sub> ratio, and CO fraction.

The equation for a quadratic model for the CH<sub>4</sub> yield is given in equation 23.

$$\begin{aligned} \text{CH}_4 \text{ Yield} = & +31 + 7.33X_1 + 0.1667X_2 + 9.75X_3 - 1.08X_4 - 2.25X_1X_2 + 11.0X_1X_3 - \\ & -3.75X_1X_4 + 4.5X_2X_3 - 0.75X_2X_4 + 1.75X_3X_4 - 2.25X_1^2 - 3.25X_2^2 - 3.87X_3^2 - 8.62X_4^2 \end{aligned} \quad (24)$$

Equations 23 and 24 in terms of actual factors can be used to make predictions about the response for given levels of each factor. To achieve this, the levels must be specified in the original units of each factor both for the input parameters and the response.

The analysis of the performance of the models is given in Table 6. For the CO<sub>2</sub> conversion, the predictive capacity of the model was high ( $R^2=0.9949$ , adjusted  $R^2=0.9922$  and predicted  $R^2=0.9835$ ).  $R^2$  values greater than 0.8 are usually an indication of a significant fit between experimental and model-predicted results. The coefficient of variance (CV) was 5.64% which is low and indicates a good reliability of the experiments.

Figure 8 shows the actual vs. predicted response for the reduced cubic regression model.

The parity plot in Figure 8a and Figure 8b shows the relationship between the actual and predicted responses corresponding to the CO<sub>2</sub> conversion and CH<sub>4</sub> yield. Figure 8a shows that the actual and predicted output response for the CO<sub>2</sub> conversion were aligned perfectly at the 45° line indicating very good regression and agreement between the two data sets. However, figure 8b shows the actual and predicted output response for the CH<sub>4</sub> yield indicating a fairly good agreement with each other although not as good as the CO<sub>2</sub> conversion response. The data points were clustered around the 45° line, however, with notable distance from the line indicating some noise, there is still an acceptable level of agreement between both data.

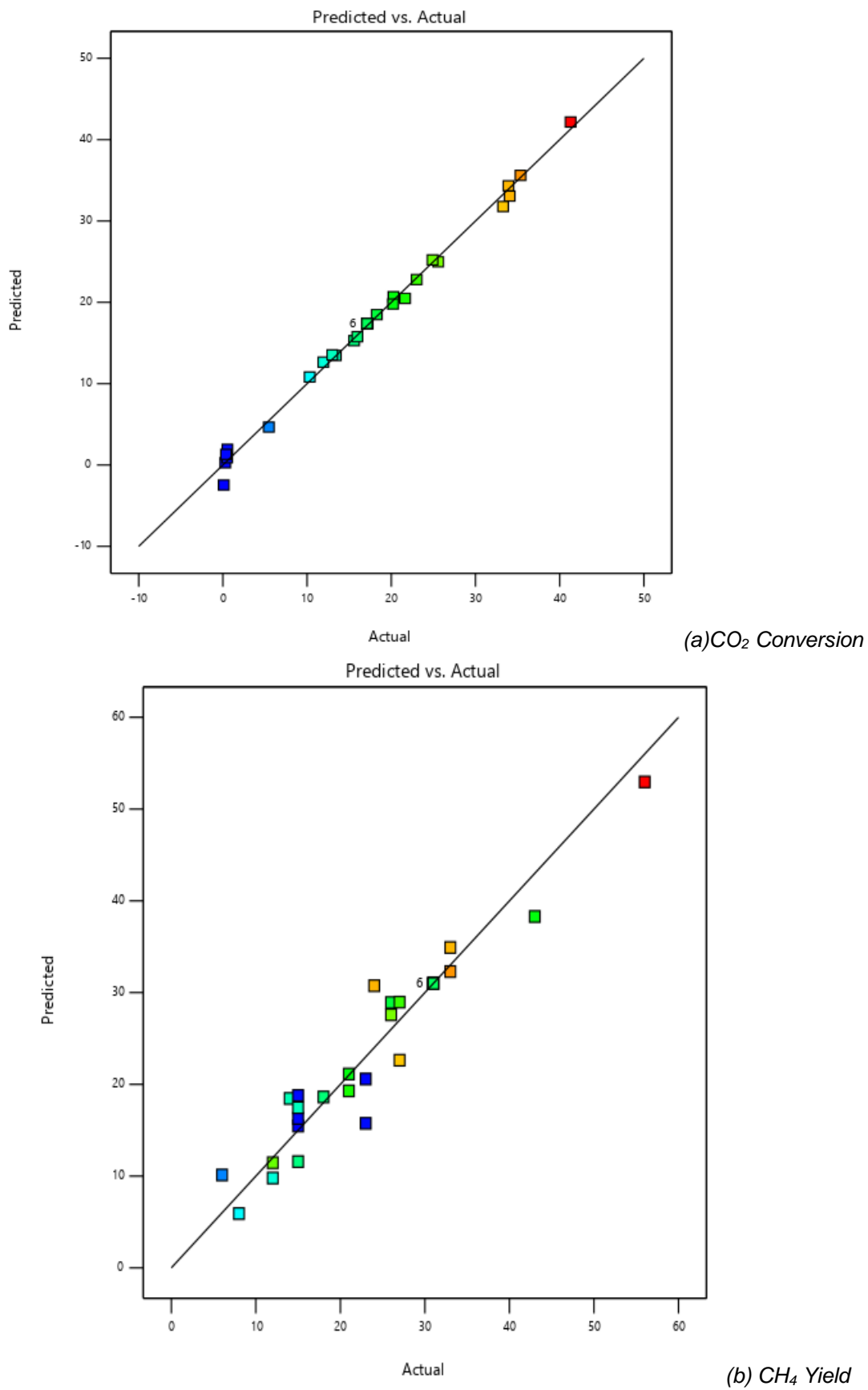


Figure 8. Parity plot of actual vs. predicted values for  $R_1$  and  $R_2$

#### 4.3. Results for ANN Modelling

The ANN neural network model was used to determine the relationship between the input factors and the output response. The selection of the best neural network for the ANN analyses was based on the performance of the best transfer functions, training algorithm, network, and optimal number of neurons. The training was performed severally and the best trained results were used to represent the model. The performance of these variables was assessed based on the  $R^2$  values, mean absolute error (MSE), root mean squared error (RMSE), mean absolute error (MAE), and

mean absolute percentage error (MAPE). The highest  $R^2$  value and the lowest MSE, RMSE, MAE, and MAPE values indicate better predictions corresponding to the modelling factors. The  $R^2$  value from the ANN model corresponding to the selected trained model is shown in Figure 9.

Figure 9 shows the  $R^2$  values corresponding to the two ANN trainings performed. The Overall  $R^2$  values for the  $\text{CO}_2$  conversion and  $\text{CH}_4$  yield training were 0.9901 and 0.98873 respectively. It is seen that ANN gave notably high  $R^2$  values which indicate very good predictions both for the  $\text{CO}_2$  conversion and the  $\text{CH}_4$  yield.

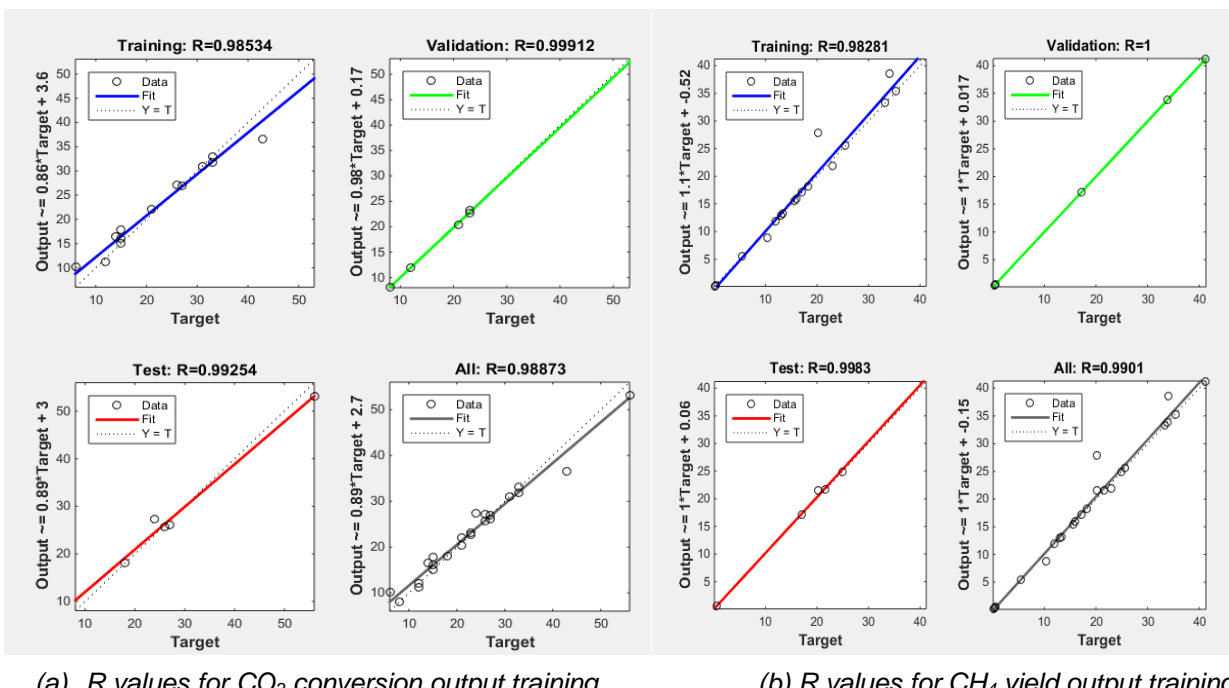


Figure 9.  $R$ -values for the training in ANN

Table 5 shows the values predicted by RSM and ANN models for each of the input variables and actual output data. Table 5 shows that there is a high correlation between the actual and predicted results for the RSM and the ANN models.

Table 5. Actual and predicted results for  $\text{CO}_2$  conversion and  $\text{CH}_4$  yield corresponding to RSM and ANN modelling

T, °C	P, bar	H <sub>2</sub> /CO <sub>2</sub> Ratio	CO fraction	Actual Data		RSM Prediction		ANN Prediction	
				CO <sub>2</sub> Conversion	CH <sub>4</sub> Yield	CO <sub>2</sub> Conversion	CH <sub>4</sub> Yield	CO <sub>2</sub> Conversion	CH <sub>4</sub> Yield
400	75	2.75	0.06	17.12	31.00	17.40	31.00	17.12	30.97
300	75	4	0.06	0.37	15.00	1.31	16.29	0.36	17.82
500	75	2.75	0	35.35	33.00	35.61	32.29	35.34	31.76
300	75	2.75	0.12	0.10	15.00	-2.46	15.46	0.10	15.06
300	100	2.75	0.06	0.28	23.00	0.27	20.58	0.30	23.19
400	75	1.5	0.12	10.31	8.00	10.82	5.92	8.81	8.06

400	100	2.75	0	20.20	21.00	19.79	21.13	27.82	20.42
400	75	2.75	0.06	17.12	31.00	17.40	31.00	17.12	30.97
400	75	4	0	25.57	26.00	24.99	27.58	25.54	27.16
500	75	4	0.06	41.30	56.00	42.17	52.96	41.21	53.08
400	50	2.75	0	21.64	21.00	20.48	19.29	21.64	22.08
500	75	2.75	0.12	33.28	27.00	31.78	22.62	33.27	26.12
500	100	2.75	0.06	34.06	24.00	33.06	30.75	38.51	27.33
300	75	2.75	0	5.46	6.00	4.67	10.13	5.47	10.16
400	75	2.75	0.06	17.12	31.00	17.40	31.00	17.12	30.97
400	75	2.75	0.06	17.12	31.00	17.40	31.00	17.12	30.97
300	50	2.75	0.06	0.53	23.00	1.93	15.75	0.54	22.74
400	50	1.5	0.06	13.41	14.00	13.46	18.46	13.19	16.46
300	75	1.5	0.06	0.52	15.00	0.89	18.79	0.51	15.06
400	75	1.5	0	15.58	15.00	15.29	11.58	15.52	15.08
400	100	2.75	0.12	12.99	15.00	13.54	17.46	12.98	16.02
400	100	4	0.06	20.25	43.00	20.69	38.29	21.54	36.60
400	50	2.75	0.12	15.97	18.00	15.77	18.63	15.96	18.03
500	75	1.5	0.06	24.90	12.00	25.21	11.46	24.92	11.19
500	50	2.75	0.06	17.12	31.00	17.40	31.00	17.12	30.97
400	75	4	0.12	0.37	15.00	1.31	16.29	0.36	17.82
400	75	2.75	0.06	35.35	33.00	35.61	32.29	35.34	31.76
400	75	2.75	0.06	0.10	15.00	-2.46	15.46	0.10	15.06
400	100	1.5	0.06	0.28	23.00	0.27	20.58	0.30	23.19
400	50	4	0.06	10.31	8.00	10.82	5.92	8.81	8.06

Table 6 shows the comparison of performance metrics for the RSM and the ANN predictions.

Table 6. Performance metrics for RSM and ANN Predictions

Parameter	ANN Model		RSM Model	
	CO <sub>2</sub> Conversion Output	CH <sub>4</sub> Yield Output	CO <sub>2</sub> Conversion Output	CH <sub>4</sub> Yield Output
MSE	2.7671	3.2951	0.6094	8.5808
RMSE	1.6635	1.8152	0.7806	2.9293
MAE	0.5498	1.0028	0.5812	2.1650
MAPE	0.0322	0.0595	1.0936	0.1244
R <sup>2</sup>	0.9901	0.9887	0.9949	0.9219

From Table 6, it is seen that both RSM and ANN models gave realistic predictions of the actual/experimental data for the error metrics considered. In terms of R<sup>2</sup> values, both RSM and ANN gave predictions higher than 0.9 which indicates very good predictions of the test data. The R<sup>2</sup> values for CO<sub>2</sub> conversion for RSM and ANN were 0.9901 and 0.9949 respectively. Thus, in terms of CO<sub>2</sub> conversion, the performance of RSM and ANN relative to R<sup>2</sup> values were almost the same with RSM surpassing ANN with minor

differences. These were within the values reported by Sun et al., (2018) in their study on optimisation of CO<sub>2</sub> hydrogenation in microchannel reactor using ANN and RSM models. However, it can be seen that ANN outperformed RSM when predicting CH<sub>4</sub> yield. This indicates that ANN is a superior predictive model for CH<sub>4</sub> yield. It should be noted that CH<sub>4</sub> yield was related to much more complex reactions that occur in the multi-tubular fixed bed reactor. The reactions that led to CH<sub>4</sub> yield comprised the RWGS reaction and CO methanation reaction as opposed to the RWGS

reaction alone which accounted for the  $\text{CO}_2$  conversion. Apparently, ANN proved a better model for handling datasets with much more complex data points than RSM.

In terms of MSE, RMSE, MAE, and MAPE, the RSM outperformed ANN for  $R_1$  prediction when considering MSE and RMSE. However, ANN modelled results showed better performance when considering MAE and MAPE. For  $R_2$  predictions, the ANN showed lower errors than RSM for all values of MSE, RMSE, MAE, and MAPE.

#### 4.5. Optimisation of $\text{CO}_2$ Conversion and $\text{CH}_4$ Yield

Table 7 gives the summary of the optimisation results for  $\text{CO}_2$  conversion and  $\text{CH}_4$  yield corresponding to RSM and ANN-GA optimisations performed.

Table 7. Optimisation results

Parameter	RSM	ANN-GA
Temperature, $^{\circ}\text{C}$	500	500
Pressure, bars	84.88	78.96
$\text{H}_2/\text{CO}_2$ ratio	4	4
CO Fraction	0.0483	0.0382
$\text{CO}_2$ Conversion, %	42.3	44.56
$\text{CH}_4$ Yield, %	57.73	58.94

From Table 7, it can be seen that for both  $\text{CO}_2$  conversion and  $\text{CH}_4$  yield, ANN-GA gave higher optimised values than RSM. For the RSM optimisation, the optimal values of temperature, pressure,  $\text{H}_2/\text{CO}_2$  ratio, and CO fraction were  $500^{\circ}\text{C}$ , 84.88 bars, 4, 0.0483 respectively while for ANN-GA optimisation, the optimised values of temperature, pressure,  $\text{H}_2/\text{CO}_2$  ratio and CO fraction were  $500^{\circ}\text{C}$ , 78.96 bars, 4 and 0.0382 respectively. The optimised values of temperature and  $\text{H}_2/\text{CO}_2$  ratio of RSM were the same as that of ANN-GA. The optimised values of pressure and CO fraction for RSM were higher than that of ANN-GA indicating that ANN-GA requires less pressure and CO fraction to be optimised. The optimised values of the  $\text{CO}_2$  conversion and  $\text{CH}_4$  yield were 42.3% and 57.73% for RSM optimisation but 44.56% and 58.94% for ANN-GA optimisation. Generally, the result shows that ANN-GA gave a better optimisation prediction than RSM.

## 5. CONCLUSIONS

A comprehensive investigation of the process simulation and optimisation of  $\text{CO}_2$  methanation for the production of synthetic natural gas (SNG) has been conducted in this study. SNG production was simulated using Aspen HYSYS software. The methanation process investigated focused on

output results such as  $\text{CO}_2$  conversion,  $\text{CH}_4$  yield, and  $\text{CH}_4$  selectivity under varying process conditions and explored the effects of temperature, pressure,  $\text{H}_2/\text{CO}_2$  ratio, and CO fraction in the feedstock on these outputs. RSM and ANN were used to model the relationship between input variables and output results which provided fitness functions that were optimised using RSM and ANN-GA. The study indicates the potential of SNG production by hydrogenation of  $\text{CO}_2$  over Ni-based catalysts.

The results revealed that temperature played a crucial role in enhancing  $\text{CO}_2$  conversion and  $\text{CH}_4$  yield. Higher temperatures favoured the endothermic RWGS reaction, leading to increased  $\text{CO}_2$  conversion. However, the balance between CO and  $\text{CO}_2$  in the feedstock (represented by the CO fraction) was found to be delicate. Excessive CO fractions hindered the methanation process, reducing both  $\text{CO}_2$  conversion and  $\text{CH}_4$  yield. Additionally, the  $\text{H}_2/\text{CO}_2$  ratio proved critical as higher ratios facilitated higher  $\text{CO}_2$  conversion,  $\text{CH}_4$  selectivity, and yield, emphasizing the significance of an optimal hydrogen-to- $\text{CO}_2$  ratio for efficient methanation.

More so, the ANN-GA model outperformed RSM in terms of prediction accuracy and optimization. The ANN-GA model demonstrated superior capabilities in capturing the complex relationships between the input variables and output responses. By leveraging the power of artificial neural networks and genetic algorithms, the ANN-GA model provided more precise and efficient predictions, offering a deeper understanding of the intricate interactions within the methanation process. The superiority of the ANN-GA model highlights the potential of advanced computational techniques in optimizing complex chemical processes.

## 6. REFERENCES

- [1] N.A.M.Razali, K.T. Lee, S. Bhatia, A.R. Mohamed (2012) Heterogeneous Catalysts for Production of Chemicals Using Carbon Dioxide as Raw Material: A Review. *Renewable Sustainable Energy Rev.* 16, 4951–4964. <https://doi.org/10.1016/j.rser.2012.04.012>.
- [2] W.Li, H. Wang, X. Jiang, J. Zhu, Z.Liu, X. Guo, C. Song (2018) A short review of recent advances in  $\text{CO}_2$  hydrogenation to hydrocarbons over heterogeneous catalysts. *RSC Adv.*, 8, 7651–7669. <https://doi.org/10.1039/C7RA13546G>.
- [3] L. Li, W. Zeng, M. Song, X. Wu, G. Li, C. Hu. (2022). Research progress and reaction mechanism of  $\text{CO}_2$  methanation over Ni-based catalysts at low temperature: A review. *Catalysts*, 12, 244. <https://doi.org/10.3390/catal12020244>

[4] M. Younas, M. Sohail, L. K. Leong, M. J. K. Bashir, H. Nadeem, S. Shehzad, S. Sumathi. (2017). Recent advancements, fundamental challenges, and opportunities in catalytic methanation of CO<sub>2</sub>. *Energy & Fuels*, 31(11), 8815–8831. <https://doi.org/10.1021/acs.energyfuels.6b01723>

[5] M. Obeid, C. Poupin, M. Labaki, S. Aouad, F. Delattre, S. Gupta, E. Abi-Aad. (2023). CO<sub>2</sub>methanation over LDH derived NiMgAl and NiMgAlFe oxides: Improving activity at lower temperatures via an ultrasound-assisted preparation. *Chemical Engineering Journal*, 474, 145460. <https://doi.org/10.1016/j.cej.2023.145460>

[6] M. Younas, L. K. Kong, M. J. Bashir, H. Nadeem, A. Shehzad, S. Sethupathi. (2016). Recent advancements, fundamental challenges, and opportunities in catalytic methanation of CO<sub>2</sub>. *Energy & Fuels*, 30(11), 8815–8831. <https://doi.org/10.1021/acs.energyfuels.6b01723>

[7] J. Wei, Q. Ge, R. Yao, Z. Wen, C. Fang, L. Guo, H. Xu, J. Sun. (2017). Directly converting CO<sub>2</sub> into a gasoline fuel. *Nature Communications*, 8(1), 15174. <https://doi.org/10.1038/ncomms15174>

[8] N. D. MohdRidzuan, M. S. Shararun, M. A. Anawar, I. Ud-Din. (2022). Ni-based catalyst for carbon dioxide methanation: A review on performance and progress. *Catalysts*, 12, 469. <https://doi.org/10.3390/catal12050469>

[9] S. Biswas, A. P. Kulkarni, S. Giddey, S. Bhattacharya. (2020). A review on synthesis of methane as a pathway for renewable energy storage with a focus on solid oxide electrolytic cell-based processes. *Frontiers in Energy Research*, 8, 570112. <https://doi.org/10.3389/fenrg.2020.570112>

[10] L. Barelli, G. Bidini, P. A. Ottaviano, M. Perla. (2021). Liquefied synthetic natural gas produced through renewable energy surplus: Impact analysis on vehicular transportation by 2040 in Italy. *Gases*, 1, 80–91. <https://doi.org/10.3390/gases1020007>

[11] K. Stangeland, D. Kalai, H. Li, Z. Yu. (2017). CO<sub>2</sub>methanation: The effect of catalysts and reaction conditions. *Energy Procedia*, 105, 2022–2027. <https://doi.org/10.1016/j.egypro.2017.03.577>

[12] A. Mazza, E. Bompard, G. Chicco. (2018). Applications of power to gas technologies in emerging electrical systems. *Renewable and Sustainable Energy Reviews*, 92, 794–806. <https://doi.org/10.1016/j.rser.2018.04.072>

[13] R. Curie. (2019). Design and Simulation of Novel Sabatier Reactors for the Thermocatalytic Conversion of CO<sub>2</sub> into Renewable Natural Gas (Master's thesis). University of Waterloo. <http://hdl.handle.net/10012/14542>

[14] A. Kolakoti, G. Satish. (2023). Biodiesel production from low-grade oil using heterogeneous catalyst: an optimisation and ANN modelling. *Australian Journal of Mechanical Engineering*, 21(1), 316–328. <https://doi.org/10.1080/14484846.2020.1842298>

[15] C. Bassano, P. Deiana, L. Lietti, C.G. Visconti. (2019). P2G movable modular plant operation on synthetic methane production from CO<sub>2</sub> and hydrogen from renewable sources. *Fuel*, 253, 1071–1079. <https://doi.org/10.1016/j.fuel.2019.05.074>

[16] C. E. Yeo, M. Seo, D. Kim, C. Jeong, H. S. Shin, S. Kim. (2021). Optimization of operating conditions for CO<sub>2</sub>methanation process using design of experiments. *Energies*, 14(24), 8414. <https://doi.org/10.3390/en14248414>

[17] A. Kolakoti, P. Bobbili, S. Katakam, S. Geeri, W. G. Soliman. (2023). Applications of artificial intelligence in sustainable energy development and utilization. In *Computational Intelligence in Sustainable Reliability Engineering* (pp. 129–143). <https://doi.org/10.1002/9781119865421.ch6>

[18] A. Z. AbHalim, R. Ali, W. A. Wan Abu Bakar. (2015). CO<sub>2</sub>/H<sub>2</sub>methanation over M<sup>\*</sup>/Mn/Fe-Al<sub>2</sub>O<sub>3</sub> (M<sup>\*</sup>: Pd, Rh, and Ru) catalysts in natural gas; optimization by response surface methodology-central composite design. *Clean Technologies and Environmental Policy*, 17, 627–636. <https://doi.org/10.1007/s10098-014-0814-8>

[19] N. Ali, M. Bilal, M. S. Nazir, A. Khan, F. Ali, H. M. Iqbal. (2020). Thermochemical and electrochemical aspects of carbon dioxide methanation: A sustainable approach to generate fuel via waste to energy theme. *Science of the Total Environment*, 712, 136482. <https://doi.org/10.1016/j.scitotenv.2019.136482>

[20] M. Younas, S. Sethupathi, L. L. Kong, A. R. Mohamed. (2018). CO<sub>2</sub>methanation over Ni and Rh based catalysts: Process optimization at moderate temperature. *International Journal of Energy Research*, 42(10), 3289–3302. <https://doi.org/10.1002/er.4082>

[21] Y. Zhang, B. Wang, Z. Ji, Y. Jiao, Y. Shao, H. Chen, X. Fan. (2023). Plasma-catalytic CO<sub>2</sub>methanation over NiFe/(Mg, Al) Ox catalysts: Catalyst development and process optimisation. *Chemical Engineering Journal*, 465, 142855. <https://doi.org/10.1016/j.cej.2023.142855>

[22] V. Dieterich, A. Buttler, A. Hanel, H. Spliethoff, S. Fendt. (2020). Power-to-liquid via synthesis of methanol, DME or Fischer–Tropsch-fuels: a review. *Energy & Environmental Science*, 13(10), 3207–3252. <https://doi.org/10.1039/D0EE01187H>

[23] J. Gao, Y. Wang, Y. Ping, D. Hu, G. Xu, F. Gu, F. Su. (2012). A thermodynamic analysis of methanation reactions of carbon oxides for the production of synthetic natural gas. *RSC Advances*, 2(6), 2358–2368. <https://doi.org/10.1039/C2RA00632D>

[24] M. F. Neubert. (2020). Catalytic methanation for small-and mid-scale SNG production. *Friedrich-Alexander-Universität Erlangen-Nürnberg*. <https://open.fau.de/handle/openfau/13118>

[25] A. El Sibai, L. Rihko-Struckmann, K. Sundmacher. (2015). Synthetic methane from CO<sub>2</sub>: Dynamic optimization of the Sabatier process for power-to-

gas applications. In Computer Aided Chemical Engineering (Vol. 37, pp. 1157–1162). Elsevier. <https://doi.org/10.1016/B978-0-444-63577-8.50038-3>

[26] L. Shen, J. Xu, M. Zhu, Y. F. Han. (2020). Essential role of the support for nickel-based CO<sub>2</sub>methanation catalysts. *ACS Catalysis*, 10(24), 14581–14591. <https://doi.org/10.1021/acscatal.0c03471>

[27] E. I. Papaioannou, S. Souentie, A. Hammad, C. G. Vayenas. (2009). Electrochemical promotion of the CO<sub>2</sub> hydrogenation reaction using thin Rh, Pt and Cu films in a monolithic reactor at atmospheric pressure. *Catalysis Today*, 146(3–4), 336–344. <https://doi.org/10.1016/j.cattod.2009.06.008>

[28] L. Jürgensen, E. A. Ehimen, J. Born, J. B. Holm-Nielsen. (2015). Dynamic biogas upgrading based on the Sabatier process: Thermodynamic and dynamic process simulation. *Bioresource Technology*, 178, 323–329. <https://doi.org/10.1016/j.biortech.2014.10.069>

[29] J. Schumacher, D. Meyer, J. Friedland, R. Güttel. (2022). Evaluation of the application of different diffusion models for the methanation of CO/CO<sub>2</sub> mixtures. *Results in Engineering*, 13, 100355. <https://doi.org/10.1016/j.rineng.2022.100355>

[30] A. Streb, M. Mazzotti. (2022). Performance limits of neural networks for optimizing an adsorption process for hydrogen purification and CO<sub>2</sub> capture. *Computers & Chemical Engineering*, 166, 107974. <https://doi.org/10.1016/j.compchemeng.2022.107974>

[31] I. Agirre, E. Acha, J. F. Cambra, V. L. Barrio. (2021). Water sorption enhanced CO<sub>2</sub>methanation process: Optimization of reaction conditions and study of various sorbents. *Chemical Engineering Science*, 237, 116546. <https://doi.org/10.1016/j.ces.2021.116546>

[32] W. L. Becker, M. Penev, R. J. Braun. (2019). Production of synthetic natural gas from carbon dioxide and renewably generated hydrogen: A techno-economic analysis of a power-to-gas strategy. *Journal of Energy Resources Technology*, 141(2), 021901. <https://doi.org/10.1115/1.4041381>

[33] R. A. Hubble, J. Y. Lim, J. S. Dennis. (2016). Kinetic studies of CO<sub>2</sub>methanation over a Ni/γ-Al<sub>2</sub>O<sub>3</sub> catalyst. *Faraday Discussions*, 192, 529–544. <https://doi.org/10.1039/C6FD00043F>

[34] J. Lefebvre, N. Trudel, S. Bajohr, T. Kolb. (2018). A study on three-phase CO<sub>2</sub>methanation reaction kinetics in a continuous stirred-tank slurry reactor. *Fuel*, 217, 151–159. <https://doi.org/10.1016/j.fuel.2017.12.082>

[35] D. Katla, D. Węcel, M. Jurczyk, A. Skorek-Osikowska. (2023). Preliminary experimental study of a methanation reactor for conversion of H<sub>2</sub> and CO<sub>2</sub> into synthetic natural gas (SNG). *Energy*, 263, 125881. <https://doi.org/10.1016/j.energy.2022.125881>

[36] M. Hervy, J. Maistrello, L. Brito, M. Rizand, E. Basset, Y. Kara, M. Maheut. (2021). Power-to-gas: CO<sub>2</sub>methanation in a catalytic fluidized bed reactor at demonstration scale, experimental results and simulation. *Journal of CO<sub>2</sub> Utilization*, 50, 101610. <https://doi.org/10.1016/j.jcou.2021.101610>

[37] M. Held, D. Schollenberger, S. Sauerschell, S. Bajohr, T. Kolb. (2020). Power-to-Gas: CO<sub>2</sub>methanation concepts for SNG production at the Engler-Bunte-Institut. *ChemieIngenieurTechnik*, 92(5), 595–602. <https://doi.org/10.1002/cite.201900181>

[38] D. L. Reddy, D. Lokhat, H. Siddiqi, B. C. Meikap. (2022). Modelling and simulating CO and CO<sub>2</sub>methanation over Ru/γ-Al<sub>2</sub>O<sub>3</sub> catalyst: An integrated approach from carbon capture to renewable energy generation. *Fuel*, 314, 123095. <https://doi.org/10.1016/j.fuel.2021.123095>

[39] T. Chwoła, T. Spietz, L. Więsław-Solny, A. Tatarczuk, A. Krótki, S. Dobras, M. Stec, J. Zdeb. (2020). Pilot plant initial results for the methanation process using CO<sub>2</sub> from amine scrubbing at the Łaziska power plant in Poland. *Fuel*, 263, 116804. <https://doi.org/10.1016/j.fuel.2019.116804>

[40] S. Rönsch, J. Schneider, S. Matthischke, M. Schlüter, M. Götz, J. Lefebvre, P. Prabhakaran, S. Bajohr. (2016). Review on methanation – From fundamentals to current projects. *Fuel*, 166, 276–296. <https://doi.org/10.1016/j.fuel.2015.10.111>

[41] H. Nam, J. H. Kim, H. Kim, M. J. Kim, S. G. Jeon, G. T. Jin, H. J. Ryu. (2021). CO<sub>2</sub>methanation in a bench-scale bubbling fluidized bed reactor using Ni-based catalyst and its exothermic heat transfer analysis. *Energy*, 214, 118895. <https://doi.org/10.1016/j.energy.2020.118895>

[42] S. I. Ngo, Y. I. Lim, D. Lee, M. W. Seo, S. Kim. (2021). Experiment and numerical analysis of catalytic CO<sub>2</sub>methanation in bubbling fluidized bed reactor. *Energy Conversion and Management*, 233, 113863. <https://doi.org/10.1016/j.enconman.2021.113863>

[43] W. J. Lee, C. Li, H. Prajitno, J. Yoo, J. Patel, Y. Yang, S. Lim. (2021). Recent trend in thermal catalytic low temperature CO<sub>2</sub>methanation: A critical review. *Catalysis Today*, 368, 2–19. <https://doi.org/10.1016/j.cattod.2020.02.017>

[44] J. Ye, Y. Yao, Y. Zhao, Q. Yang, L. Ma, W. Zhang, C. Tang. (2021). A review of CO<sub>2</sub>methanation: Key factors of catalyst, mechanism, and process. *Frontiers in Energy Research*, 9, 694805. <https://doi.org/10.3389/fenrg.2021.694805>

[45] K. Nawaz, M. Sohail, M. A. Naz. (2021). Recent developments in catalytic CO<sub>2</sub>methanation: A review. *Environmental Science and Pollution Research*, 28, 31960–31984. <https://doi.org/10.1007/s11356-021-13166-1>

[46] M. Z. K. Kamarudin, S. L. Lee, M. S. M. Nor. (2021). CO<sub>2</sub> hydrogenation to methane: Recent advances in catalyst development and reaction mechanisms. *Renewable and Sustainable Energy Reviews*, 135, 110177. <https://doi.org/10.1016/j.rser.2020.110177>

## IZVOD

### METODOLOGIJA POVRŠINE ODZIVA I OPTIMIZACIJA VEŠTAČKIH NEURONSKIH MREŽA ZA SIMULACIJU METANACIJE $\text{CO}_2$ KORIŠĆENJEM $\text{Ni}/\text{MgAl}_2\text{O}_4$ KATALIZATORA U VIŠECEVNOM REAKTORU SA FIKSNIOM SLOJEM

Ova studija je istraživala simulaciju i optimizaciju proizvodnje sintetičkog metana preko  $\text{Ni}/\text{MgAl}_2\text{O}_4$  u višecevnom reaktoru sa fiksniom slojem. Studija obuhvata simulaciju procesa sprovedenu korišćenjem softvera Aspen HYSYS, modeliranje i optimizaciju korišćenjem metodologije površine odziva (RSM) i modeliranje veštačkih neuronskih mreža (ANN) korišćenjem softvera Design Experts i MATLAB, respektivno. U simulaciji procesa za metanaciju  $\text{CO}_2$ , izvršene su analize osetljivosti kako bi se utvrdili efekti temperature, pritiska, odnosa  $\text{H}_2/\text{CO}_2$  i frakcije CO u sirovini na konverziju  $\text{CO}_2$ , prinos  $\text{CH}_4$  i selektivnost  $\text{CH}_4$ . RSM i ANN modeli su izgrađeni korišćenjem podataka dobijenih rezultatima simulacije procesa za modeliranje odnosa između ulaznih promenljivih i izlaznih odgovora i izvršenje optimizacije za RSM model i ANN model zajedno sa genetskim algoritmom (GA). Rezultati simulacije procesa su duboko istakli uticaj temperature na povećanje konverzije  $\text{CO}_2$  i prinosa  $\text{CH}_4$ . Više temperature su favorizovale endotermnu obrnutu reakciju pretvaranja vode u gas (RWGS), što je dovelo do povećane konverzije  $\text{CO}_2$  i prinosa  $\text{CH}_4$ . Utvrđeno je da su konverzija  $\text{CO}_2$ , selektivnost  $\text{CH}_4$  i prinos minimalno pogodjeni pritiskom. Utvrđeno je da frakcija CO u dovodu ima delikatan uticaj na konverziju  $\text{CO}_2$  i prinos  $\text{CH}_4$ . Prekomerna frakcija CO je ometala proces metanacije, smanjujući i konverziju  $\text{CO}_2$  i prinos  $\text{CH}_4$ . Pored toga, odnos  $\text{H}_2/\text{CO}_2$  se pokazao kritičnim jer su viši odnosi olakšavali veću konverziju  $\text{CO}_2$ , selektivnost  $\text{CH}_4$  i prinos, naglašavajući značaj optimalnog odnosa vodonika i  $\text{CO}_2$  za efikasnu metanaciju, za koji je predloženo da bude na vrednostima višim od stehiometrijske vrednosti od 4:1. Štaviše, ANN-GA model je nadmašio RSM u pogledu tačnosti predviđanja i optimizacije. Model veštačkih neurona (ANN) pokazao je superiorne mogućnosti u obuhvatanju složenih odnosa između ulaznih promenljivih i izlaznih odgovora, što su demonstrirale metrike performansi, uključujući  $R^2$  vrednosti, MSE, RMSE itd. Rezultati optimizacije ANN-GA modela pružili su preciznija i efikasnija predviđanja u poređenju sa RSM, nudeći dublje razumevanje složenih interakcija unutar procesa metanacije.

**Ključne reči:** Veštačke neuronske mreže, metanacija  $\text{CO}_2$ , HYSYS modeliranje, metodologija površine odziva, obrnuto prebacivanje vodenog gasa, Izražavanje brzine Langmuir-Hinshelwood-Hougen-Watson

Naučni rad

Rad primljen: 11.11.2024.

Rad prihvaćen: 06.01.2025.

Ndubuisi Chimezie Nwachukwu:

Nil

Nnaemeka Princewill Ohia:

<https://orcid.org/0000-0002-4219-7062>

Stanley Toochukwu Ekwueme:

<https://orcid.org/0000-0003-3446-0905>